



The Pan-Pacific Planet Search. VII. The Most Eccentric Planet Orbiting a Giant Star

Robert A. Wittenmyer^{1,2}, M. I. Jones^{3,10}, Jonathan Horner^{1,2}, Stephen R. Kane⁴, J. P. Marshall^{1,5}, A. J. Mustill⁶, J. S. Jenkins⁷, P. A. Pena Rojas⁷, Jinglin Zhao², Eva Villaver⁸, R. P. Butler⁹, and Jake Clark¹

¹University of Southern Queensland, Computational Engineering and Science Research Centre, Toowoomba, Queensland 4350, Australia; rob.w@usq.edu.au

²Australian Centre for Astrobiology, UNSW Australia, Sydney 2052, Australia

³European Southern Observatory, Alonso de Córdova 3107, Casilla 19001, Santiago, Chile

⁴Department of Earth Sciences, University of California, Riverside, CA 92521, USA

⁵Academia Sinica, Institute of Astronomy and Astrophysics, Taipei 10617, Taiwan

⁶Departamento de Astronomía, Universidad de Chile, Casilla 36-D, Santiago, Chile

⁷Lund Observatory, Department of Astronomy & Theoretical Physics, Lund University, Box 43, SE-221 00 Lund, Sweden

⁸Departamento Física Teórica, Facultad de Ciencias, Universidad Autónoma de Madrid, Cantoblanco, E-28049, Madrid, España, Spain

⁹Department of Terrestrial Magnetism, Carnegie Institution of Washington,

5241 Broad Branch Road, NW, Washington, DC 20015-1305, USA

Received 2017 July 3; revised 2017 November 3; accepted 2017 November 4; published 2017 December 4

Abstract

Radial velocity observations from three instruments reveal the presence of a $4 M_{\text{Jup}}$ planet candidate orbiting the K giant HD 76920. HD 76920b has an orbital eccentricity of 0.856 ± 0.009 , making it the most eccentric planet known to orbit an evolved star. There is no indication that HD 76920 has an unseen binary companion, suggesting a scattering event rather than Kozai oscillations as a probable culprit for the observed eccentricity. The candidate planet currently approaches to about four stellar radii from its host star, and is predicted to be engulfed on a ~ 100 Myr timescale due to the combined effects of stellar evolution and tidal interactions.

Key words: planetary systems – stars: evolution – stars: individual (HD 76920) – techniques: radial velocities

1. Introduction

Prior to the dawn of the exoplanet era, astronomers felt that they understood how other planetary systems would look, and how the solar system formed (e.g., Lissauer 1993, and references therein). They expected to find rocky, telluric worlds, in the inner reaches of planetary systems, with gas giants further out. They expected planetary systems to be co-planar, or close to it, and that the planets they would find would move on low-eccentricity orbits. All of these ideas were based on our knowledge of the one planetary system that we knew at that time—the solar system.

With the discovery of the first planet around a Sun-like star, 51 Peg (Mayor & Queloz 1995), these assumptions began to fall around us. The first of many hot-Jupiters (e.g., Gaudi et al. 2005; Wright et al. 2012; Knutson et al. 2014), 51 Pegasi b was the antithesis of our own planetary system—a giant, Jupiter-mass planet practically skimming the surface of its host star. And as the exoplanet era proceeded, new discoveries continued to shatter our old assumptions, revealing that the diversity of planetary systems is far greater than we could ever have imagined. Some systems contain planets whose orbits are highly inclined, or even retrograde, with respect to their host’s equatorial plane (e.g., Triaud et al. 2010; Addison et al. 2013; Huber et al. 2013). Others contain planets far denser than those in the solar system (e.g., Bakos et al. 2011; Marcy et al. 2014; Sinukoff et al. 2016), or far fluffier (e.g., Anderson et al. 2011; Masuda 2014; Pepper et al. 2017). Many systems contain planets unlike anything found around the Sun, with so-called “super-Earths” and “sub-Neptunes” proving to be common in the cosmos (Howard et al. 2010; Lopez & Fortney 2014; Rogers 2015; Wolfgang & Lopez 2015). There is even growing evidence of a large population of “free-floating planets,” interstellar vagabonds roaming the depths of space (Lucas & Roche 2000; Sumi et al. 2011; Liu et al. 2013). And then there

are the eccentric planets—bodies moving on orbits more akin to the solar system’s comets than its planets (e.g., Naef et al. 2001; Tamuz et al. 2008; Kane et al. 2016)

A significant fraction of these discoveries have relied on radial velocity observations, which are required in order to estimate the minimum mass of newly discovered planets. In the first decade of the exoplanet era, the radial velocity technique was by far the most effective tool for the discovery of exoplanets, as well as their characterization, and it remains the principal method by which systems that truly resemble the solar system (with distant, massive planets) can be discovered, and thence the true frequency of solar system analogues determined (e.g., Wittenmyer et al. 2011b; Endl et al. 2016; Wittenmyer et al. 2016a, 2017a). While the radial velocity technique is an excellent tool for the detection and characterization of planets around solar-type and late-type stars, it cannot be used to search for planets around massive, early-type stars. As such, while the occurrence of planets around low-mass stars is now becoming well-established out to relatively large orbital radii, the frequency and distribution of planets around more massive stars remains an open and fascinating question (e.g., Johnson et al. 2010).

In order to learn more about the occurrence and properties of planets around more massive stars, several teams have begun surveys of “retired A-stars.” Over the past few years, such surveys have begun to bear fruit, with a number of massive planets being found (e.g., Johnson et al. 2007, 2011; Jones et al. 2011; Niedzielski et al. 2015; Reffert et al. 2015; Wittenmyer et al. 2016b). As a result, we are now beginning to understand the relationship between stellar mass and the abundance of giant planets—with strong indications that giant planets are more efficiently formed around more massive stars (e.g., Maldonado et al. 2013; Reffert et al. 2015; Jones et al. 2016; Wittenmyer et al. 2017b).

In this paper, we report the discovery of a highly eccentric planet orbiting the evolved star HD 76920. In Section 2, we

¹⁰ ESO Fellow.

detail our observations and describe the stellar properties of HD 76920. In Section 3, we detail the orbit fitting process and provide the parameters of the newly detected companion, before presenting and discussing our conclusions in Section 4.

2. Observations and Data Reduction

Observations of HD 76920 were obtained with three different high-resolution spectrographs, namely UCLES (Diego et al. 1990), at the 3.9 m Anglo-Australian Telescope, CHIRON (Tokovinin et al. 2013) installed at the 1.5 m telescope in Cerro Tololo, and FEROS (Kaufer et al. 1999), at the 2.2 m telescope in La Silla. Both UCLES and CHIRON use an iodine cell, which is placed in the stellar light path, superimposing a rich absorption line spectrum, which is used to compute a precise wavelength reference (Valenti et al. 1995; Butler et al. 1996). On the other hand, FEROS is equipped with two fibers, to simultaneously record the stellar spectrum (in the science fiber) and a ThAr lamp spectrum (in the sky fiber), from which the nightly instrumental drift can be subtracted (Baranne et al. 1996). The UCLES data reduction and radial velocity computation method is described in Butler et al. (1996) and Tinney et al. (2001). The CHIRON data were extracted and calibrated with the pipeline offered by the CHIRON team, while the radial velocities were computed using the method described in Jones et al. (2017). Finally, the extraction and calibration of the FEROS data was performed with the CERES code (Brahm et al. 2017), and the radial velocities were obtained using the method presented in Jones et al. (2017). The radial velocities from all three instruments are given in Table 1.

Stellar properties for HD 76920 were derived from iodine-free template UCLES spectra with $R \sim 60,000$, as described fully in Wittenmyer et al. (2016c). In brief, spectroscopic stellar parameters were determined via a standard one-dimensional, local thermodynamic equilibrium (LTE) abundance analysis using the 2013 version of MOOG (Snedden 1973) with the ODFNEW grid of Kurucz ATLAS9 model atmospheres (Castelli & Kurucz 2004). Complete stellar parameters from Wittenmyer et al. (2016c) and other literature sources are given in Table 2.

3. Data Analysis and Companion Parameters

3.1. Orbit Fitting

The AAT/UCLES data for HD 76920 are relatively constant, save for two observations nearly 300 m s^{-1} higher on 2010 January 29/30. These spectra were of similar S/N to the others for this target, and the observing conditions were typical, ruling out the possibility of observer error or systematic errors (e.g., scattered moonlight) for the aberrant velocities. Reprocessing the spectra through an independent reduction and Doppler pipeline gave similar results, ruling out errors in data reduction or barycentric correction. We attempted a single highly eccentric planet fit using the genetic algorithm employed by our team for other Pan-Pacific Planet Search (PPPS) data sets with sparse sampling (e.g., Wittenmyer et al. 2011a, 2015, 2017b). We searched a period range of 100–1000 days and allowed eccentricities up to $e = 0.9$, running for 50,000 iterations (about 10^7 possible configurations). The best-fit solution had a high eccentricity and a period of ~ 420 days.

Our team obtained access to CHIRON in 2015 for follow-up of interesting candidates from the PPPS, and HD 76920 was

Table 1
Radial Velocities for HD 76920

BJD-2400000	Velocity (m s^{-1})	Uncertainty (m s^{-1})	Instrument
54867.07428	17.9	2.2	AAT
55226.21880	269.5	5.3	AAT
55227.20104	303.4	3.7	AAT
55318.89227	1.0	1.9	AAT
55602.04422	6.1	1.9	AAT
55880.22005	-55.3	2.3	AAT
55906.11204	-31.3	1.8	AAT
55907.19640	-28.1	2.6	AAT
55969.07596	-15.5	2.1	AAT
56088.86366	54.1	3.8	AAT
56344.02991	-3.1	2.7	AAT
56374.98803	-16.4	2.4	AAT
56376.95955	-14.1	2.4	AAT
56377.96197	-25.2	2.6	AAT
56399.96882	-18.5	3.1	AAT
56530.31941	11.0	3.0	AAT
56744.98572	-7.3	2.4	AAT
57306.82770	311.8	4.4	CHIRON
57324.78910	36.3	4.5	CHIRON
57365.78950	-14.1	4.1	CHIRON
57433.69900	-44.8	3.6	CHIRON
57433.71310	-47.5	3.4	CHIRON
57433.72720	-41.0	3.4	CHIRON
57458.68830	-34.6	3.3	CHIRON
57458.70240	-43.8	3.7	CHIRON
57458.71650	-43.6	3.6	CHIRON
57478.64630	-27.8	4.1	CHIRON
57478.66040	-28.5	3.7	CHIRON
57478.67450	-22.3	3.7	CHIRON
57641.91300	-36.9	5.0	FEROS
57643.90570	-24.2	5.4	FEROS
57700.84340	23.1	5.9	FEROS
57702.86840	20.3	4.3	FEROS
57703.79730	32.8	4.9	FEROS
57705.85330	38.2	5.0	FEROS
57894.56040	-30.7	6.2	FEROS
57895.46980	-22.7	5.5	FEROS

Note. The velocities shown are relative to instrument-specific zero points, which are free parameters in the fitting process and are given in Table 3.

Table 2
Stellar Parameters for HD 76920

Parameter	Value	References
Spec. Type	K1 III	Houk & Cowley (1975)
Distance (pc)	184.8 ± 7.5	Gaia Collaboration et al. (2016)
$(B - V)$	1.11 ± 0.02	Høg et al. (2000)
$E(B - V)$	0.0248	...
A_V	0.0769	...
Mass (M_\odot)	1.17 ± 0.20	Wittenmyer et al. (2016c)
[Fe/H]	-0.11 ± 0.10	Wittenmyer et al. (2016c)
T_{eff} (K)	4698 ± 100	Wittenmyer et al. (2016c)
	4748	McDonald et al. (2012)
	4744	Bailer-Jones (2011)
$\log g$	2.94 ± 0.15	Wittenmyer et al. (2016c)
Radius (R_\odot)	7.47 ± 0.6	Wittenmyer et al. (2016c)
Luminosity (L_\odot)	24.0	Wittenmyer et al. (2016c)
	21.7	McDonald et al. (2012)
Age (Gyr)	7.10	Wittenmyer et al. (2016c)

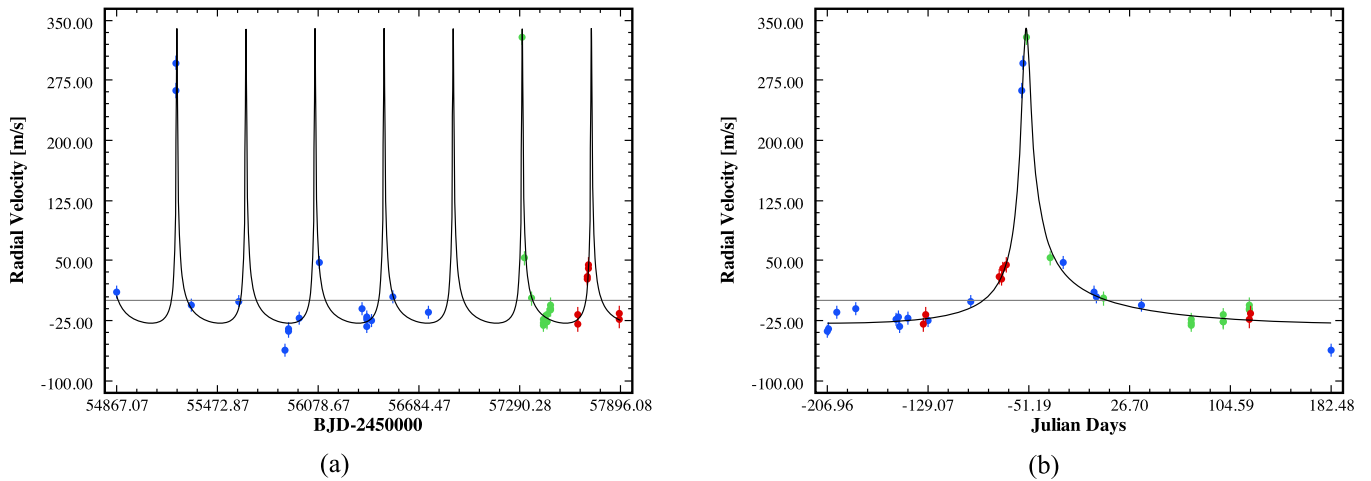


Figure 1. Data and Keplerian fit for HD 76920b (AAT—blue, CHIRON— green, FEROS—red). Error bars include 7 m s^{-1} of jitter added in quadrature. The rms about this fit is 9.74 m s^{-1} . Right: same, but phase folded on the orbital period $P = 415.4$ days.

put in the queue to catch the next predicted large velocity excursion of 2015 October. We were fortunate to catch the peak and the drop-off, confirming the period at 415 days. FEROS observations were also added and corroborated the orbit fit obtained from AAT and CHIRON. For the final fitting process, we used the Keplerian model in the *Systemic Console* version 2.2000 (Meschiari et al. 2009). For all orbit fitting, 7 m s^{-1} of jitter (excess white noise) has been added in quadrature to the internal instrumental uncertainties of each data set. This estimate is derived from the velocity scatter of 37 stable stars in the PPPS as first described in Wittenmyer et al. (2016b). While correlated noise is known to affect radial velocity data (Baluev 2013; Feng et al. 2017), we find that a white noise model is favored for all three data sets. The Bayes factors for a first-order moving average noise model (“MA(1)”) are as follows: AAT—2.3; FEROS—1.5; CHIRON—−1.7. The data and best-fit model are shown in Figure 1. Uncertainties in the system parameters were obtained with the Markov Chain Monte Carlo tool within *Systemic*. The normalized probability density functions for key parameters, resulting from a chain of 10^7 steps, are shown in Figure 2. The best fit to the data results in a planet with $P = 415.4 \pm 0.2$ days, $m \sin i = 3.93 \pm 0.15 M_{\text{Jup}}$, and $e = 0.856 \pm 0.009$ (Table 3). There is no evidence for additional Keplerian signals or velocity trends that might indicate a distant massive companion, as shown in Figure 5.

3.2. Bayesian Approach

As a further test of the validity of the detected signal in the time series, we also ran the Exoplanet Mcmc Parallel t Empering Radial velOcity fitter (EMPEROR; J. Jenkins & P. A. Pena 2017, in preparation¹¹) code to determine if the parameter estimations were robust. EMPEROR employs thermodynamic integration methods (Gregory 2005) following an affine invariant MCMC engine, performed using the EMCEE package (Foreman-Mackey et al. 2013) in Python. Correlated noise in the measurements are taken care of within EMPEROR by using a first-order moving average model, an approach that has been shown to robustly detect small amplitude signals with various morphologies and across numerous radial velocity data sets

(e.g., Jenkins et al. 2013, 2017; Tuomi et al. 2013; Jenkins & Tuomi 2014). Model selection is performed automatically by EMPEROR, whereby a Bayes Factor of five is required, a threshold probability of 150 that the more complex model is favored over the less complex one. The code also automatically determines which of the signal parameters, such as period and amplitude, are statistically significantly different from zero, and some basic priors are applied to those parameters whereby all are assumed to be flat except for the eccentricity and jitter priors that are folded Gaussian and Jeffries priors, respectively.

Under the aforementioned constraints, EMPEROR found two statistically significant signals in the radial velocity time series. The primary signal was found to be the planet signal at $415.59^{+0.19}_{-0.22}$ days, with an amplitude and eccentricity of $177.5^{+6.4}_{-3.8} \text{ m s}^{-1}$ and $0.859^{+0.005}_{-0.005}$, respectively. This result highlights the robustness of the planet detection result, showing that a long chain ($\times 10^7$) MCMC analysis to probe the posterior parameter space, along with Bayesian selection criteria, can place hard constraints on the planet signal detection and the orbital characteristics of the planet. For completeness, we show a corner plot of the posterior distribution in Figure 6.

The EMPEROR analysis found a secondary signal, which we discuss briefly here. A comparison of evidence is given in Table 4. This second signal was found with a period of $28.4^{+0.04}_{-0.57}$ days and an amplitude of $11.1^{+1.5}_{-1.5} \text{ m s}^{-1}$. The amplitude is at the level expected for the jitter of HD 76920: allowing the excess white noise (“jitter”) to vary in the single-planet model, we obtained the following for each instrument: AAT— $10.4 \pm 1.5 \text{ m s}^{-1}$, CHIRON— $8.3 \pm 1.6 \text{ m s}^{-1}$, FEROS— $2.9 \pm 1.9 \text{ m s}^{-1}$. Hence, this secondary signal is likely to originate from an intrinsic stellar process; attributing the periodicity of the secondary signal to a planet implies an orbit that crosses that of HD 76920b. Crossing orbits are almost certainly a recipe for dynamical disaster, with catastrophic instabilities occurring on timescales of a few years (e.g., Horner et al. 2011, 2013; Wittenmyer et al. 2013a; Hinse et al. 2014).

3.3. Stellar Activity

As a matter of course for new planet discoveries, we searched for activity-related signals in the spectra and publicly available photometry. Examination of 8.8 years (1403 epochs) of All-Sky Automated Survey (ASAS) photometry (Pojmanski 1997) shows

¹¹ <https://github.com/ReddTea/astroEMPEROR>

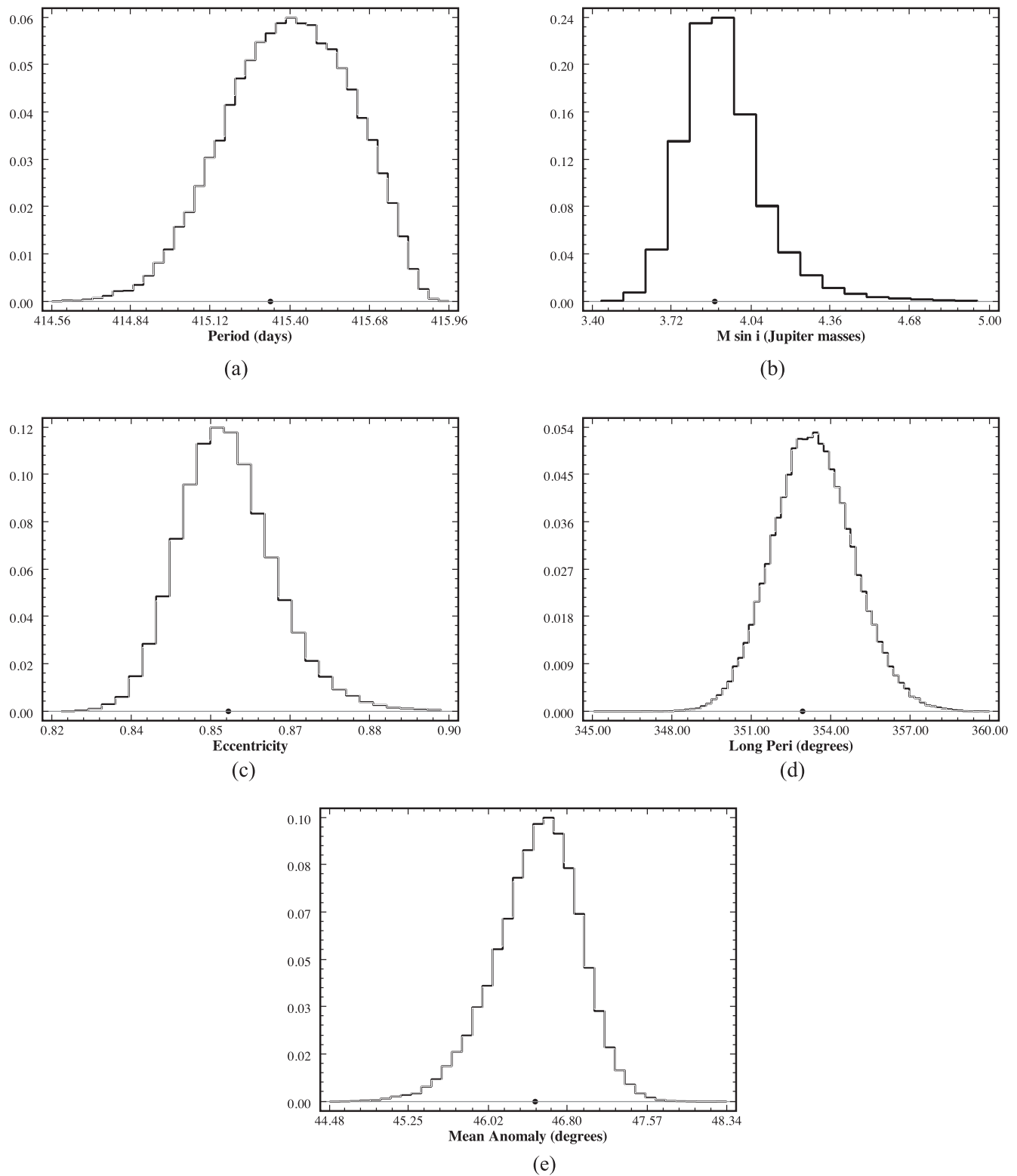


Figure 2. Posterior distributions from MCMC analysis of the combined data for HD 76920.

no periodicities of significance near the planet’s orbital period (Figure 7). The ASAS V -band photometry has a mean value of 7.827 ± 0.013 mag. We also investigated the variability in the $H\alpha$ line for our 17 AAT spectra. Variable levels of chromospheric activity can produce changes in the level of line profile reversal in some line cores, resulting in changes to the line centroid and hence the measured radial velocity (Martínez-Arnáiz

et al. 2010). These effects will also produce changes in the line’s equivalent width (EW), and so measurement of the EW can provide an indicator of the presence of activity-induced radial velocity variations (Robertson et al. 2014). Figure 8 shows the stacked spectra of HD 76920 and the radial velocity as a function of the $H\alpha$ EW. No correlation is evident: the two velocity extrema, obtained on consecutive days, have quite different EW,

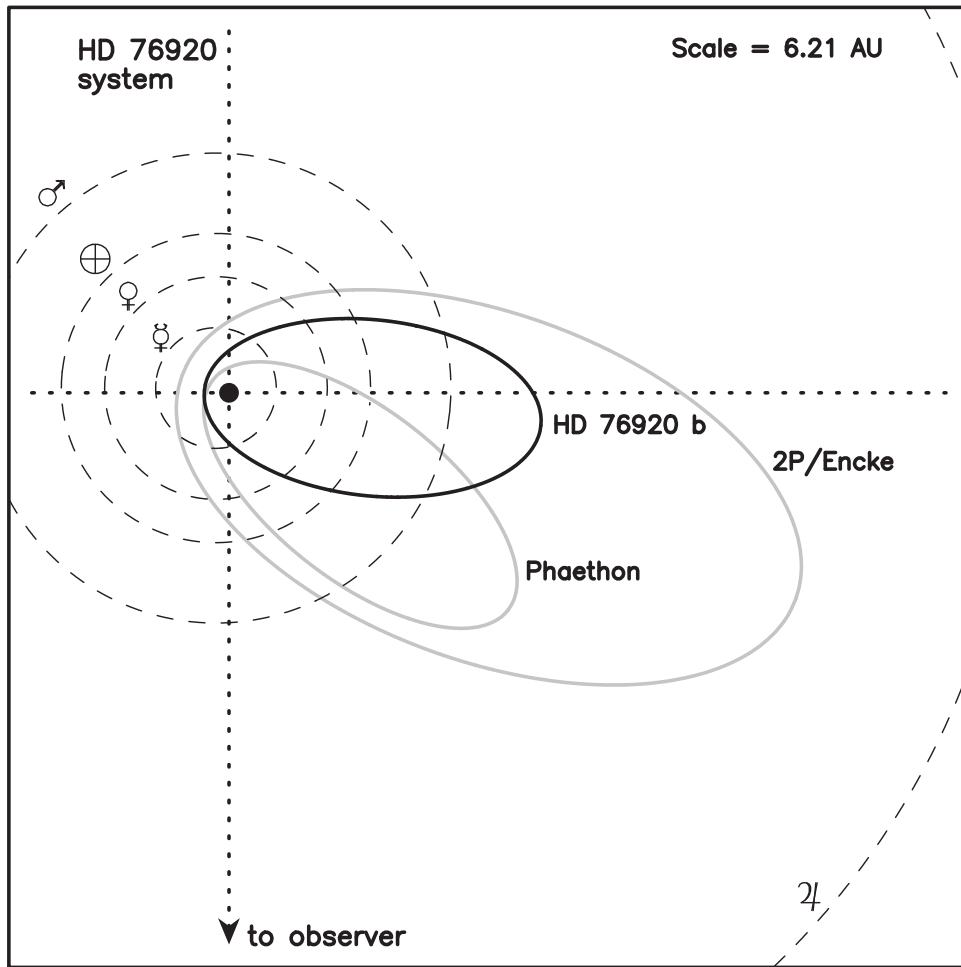


Figure 3. Orbit of HD 76920b, oriented properly and overlaid with the solar system inner planets’ orbits to scale. Comet 2P/Encke and asteroid 3200 Phaethon are shown as examples of comparably eccentric solar system bodies.

Table 3
Keplerian Orbital Solution for HD 76920b

Parameter	Value
Period (days)	415.4 ± 0.2
Eccentricity	0.856 ± 0.009
ω (degrees)	$352.9^{+1.9}_{-1.1}$
Mean anomaly ^a (degrees)	46.5 ± 0.4
K (m s^{-1})	186.8 ± 7.0
$m \sin i$ (M_{Jup})	$3.93^{+0.14}_{-0.15}$
a (au)	1.149 ± 0.017
rms about fit (m s^{-1})	9.74
Zero point—AAT m s^{-1}	7.0 ± 3.6
Zero point—CHIRON m s^{-1}	-23.7 ± 4.9
Zero point—FEROS m s^{-1}	-13.5 ± 4.7

Note.

^a At epoch BJD 2454867.07428.

one of which is consistent with the EW of the remaining spectra. Lest this discrepancy raises concerns about the candidate planetary signal, we perform one final test: Figure 9 shows the periodogram of our data with all three “high” velocities removed. The highest peak remains at 413 days with a false-alarm probability of 0.6%.

4. Discussion and Conclusions

With $e = 0.85$, HD 76920b claims the title of the most eccentric planet known to orbit a giant star (i.e., with $\log g < 3.5$). The previous record holder, iota Dra b, has $e = 0.71$ (Butler et al. 2006). To illustrate how extreme the orbit of HD 76920b is, and how dramatically different it is to the planets in our own solar system, it is useful to plot the planet’s orbit alongside the inner solar system. In Figure 3, we show how the orbit of HD 76920b compares to those of the telluric planets (Mercury, Venus, Earth, and Mars), shown to scale. In addition, we include two of the solar system’s most famous small bodies—comet 2P/Encke (the parent of the Beta Taurid and Taurid meteor streams Steel et al. 1991) and asteroid 3200 Phaethon (the parent of the Geminid meteor stream Williams & Wu 1993). Both of these objects move on dynamically unstable orbits and are only transient visitors to the inner solar system. Comet Encke is a Jupiter-family comet, and was most likely injected to its current orbit from the Centaur population—icy bodies beyond the orbit of the giant planet (e.g., Horner et al. 2003, 2004; Levison et al. 2006). 3200 Phaethon is a near-Earth asteroid, with an origin in the asteroid belt, interior to the orbit of Jupiter (e.g., de León et al. 2010). In both cases, it is clear that the objects did not form on their current orbits, but were instead transferred there from more distant, more circular orbits as a result of a lengthy series of gravitational

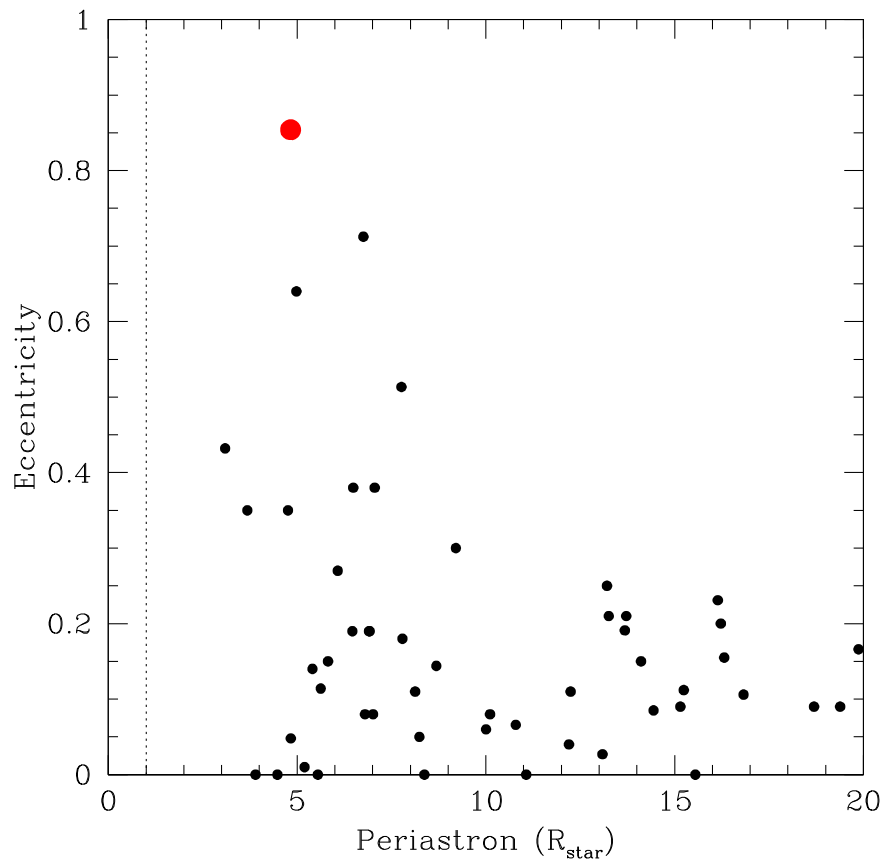


Figure 4. Orbital eccentricity vs. the planet’s periastron distance, in terms of each planet’s host-star radius, for 116 confirmed planets orbiting giant stars ($\log g < 3.5$). HD 76920b, the most eccentric such planet, is shown as a large red point.

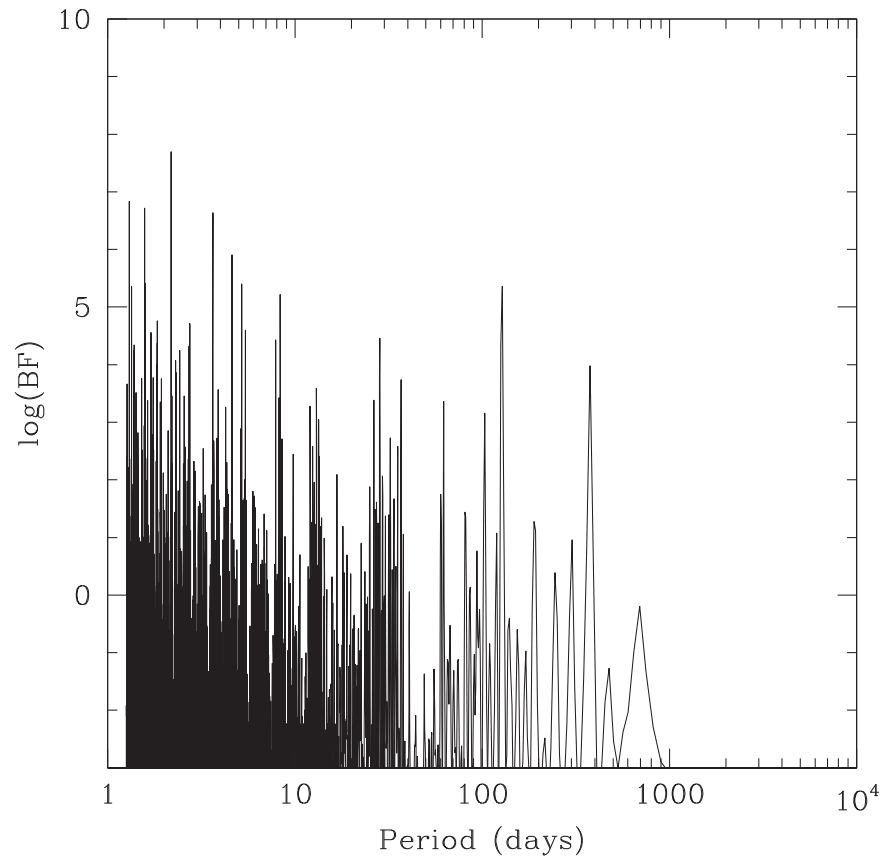


Figure 5. Bayes Factor periodogram of the residuals to our 1-planet fit. No further periodicities of interest are evident.

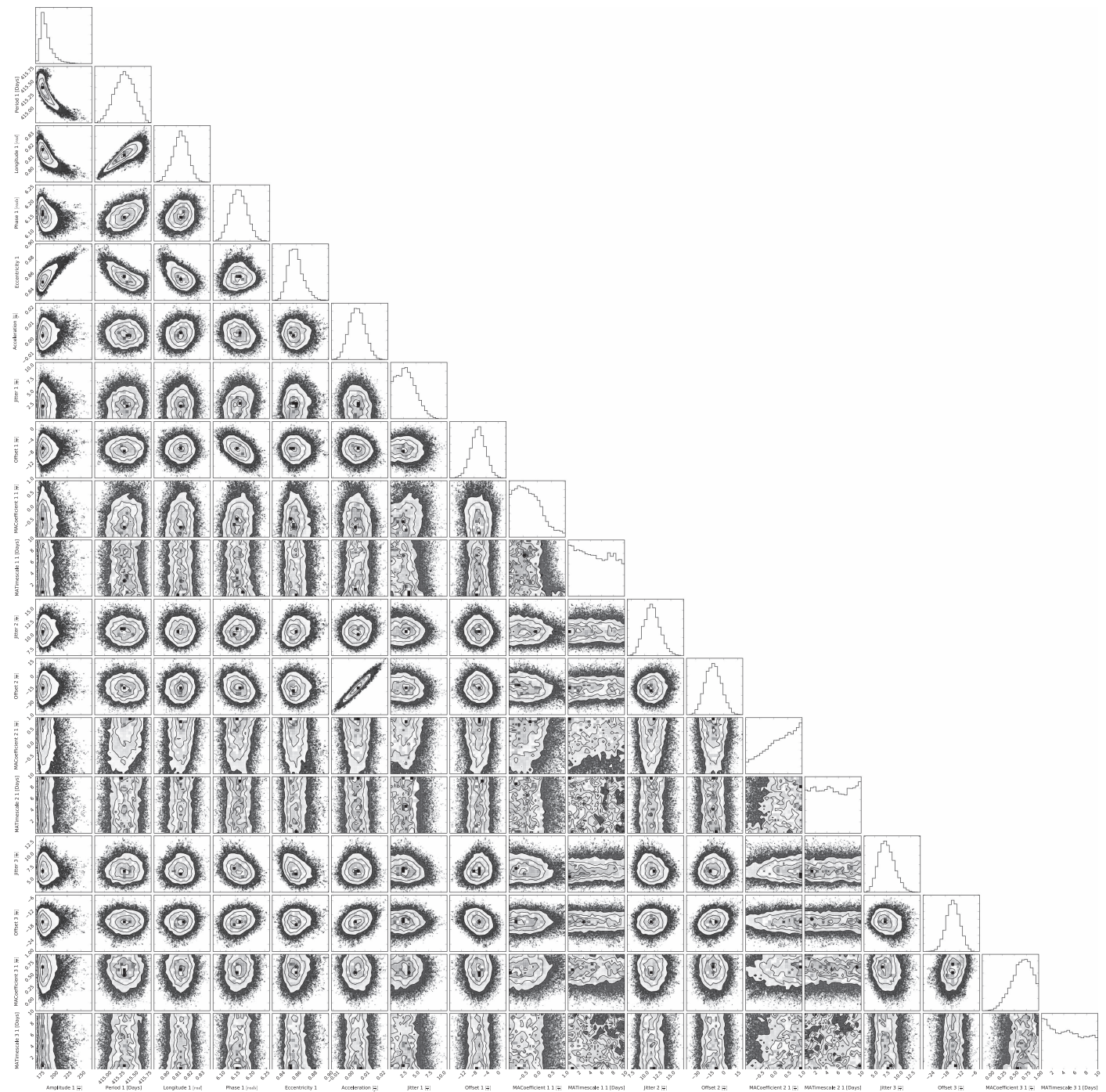


Figure 6. Corner plot of the posterior distributions from the EMPEROR results for HD 76920 single-planet fit. These results are consistent with those obtained with *Systemic*.

Table 4
Habitable Zone Boundaries for Planet Candidate Host Stars

Signals	BIC	Δ BIC (k,k-1)
k = 0	587.61	...
k = 1	319.85	267.76
k = 2	299.21	20.64

perturbations. Where non-gravitational or secular perturbations are involved (as is the case for both comet 2P/Encke and asteroid 3200 Phaethon), it is possible for the perturbed body to “decouple” from the more distant perturber, such that it no

longer undergoes periodic close encounters that can dramatically alter its orbit. Given the tidal interactions that are likely occurring between HD 76920b and its host star, there is clearly the potential for a similar process to be occurring in the HD 76920 system—with the newly discovered planet having tidally decoupled from a distant perturber and then injected to its current highly eccentric orbit.

Figure 4 shows the periastron distance for 116 confirmed planets¹² orbiting giant stars, as a function of each planet’s host-star radius. We note that the distinct absence of planets in

¹² <http://exoplanets.org>, accessed 2017 May.

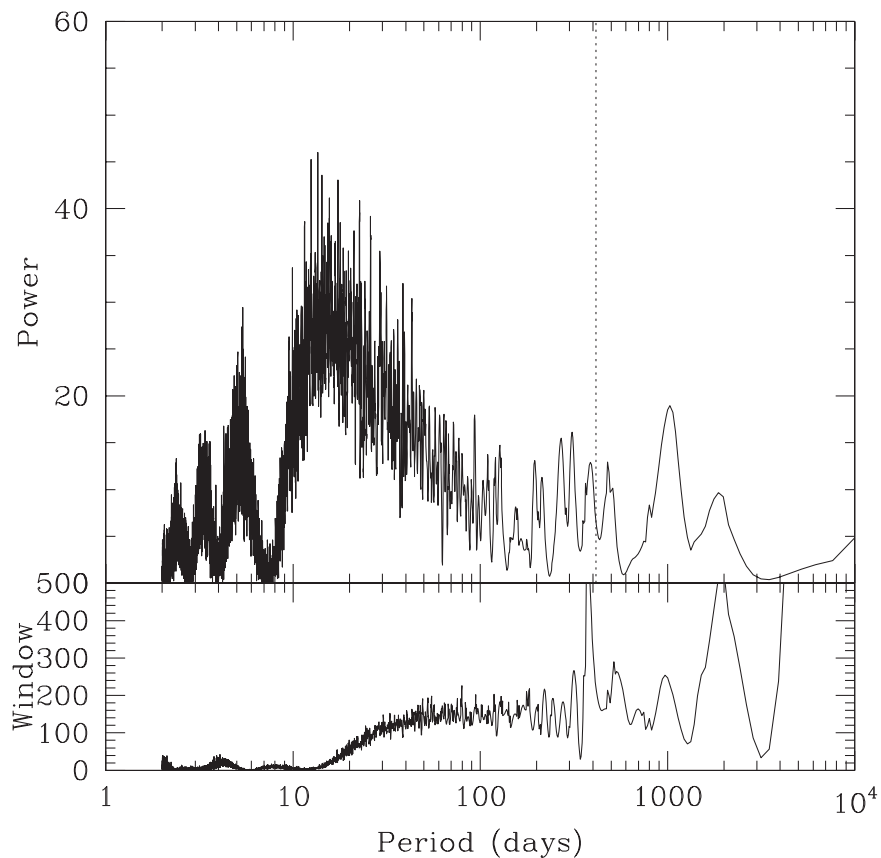


Figure 7. Generalised Lomb–Scargle periodogram of ASAS photometry for HD 76920. A total of 1403 epochs spanning 8.8 years yield no significant periodicities. The 415 day period of the planet is marked with a dotted line.

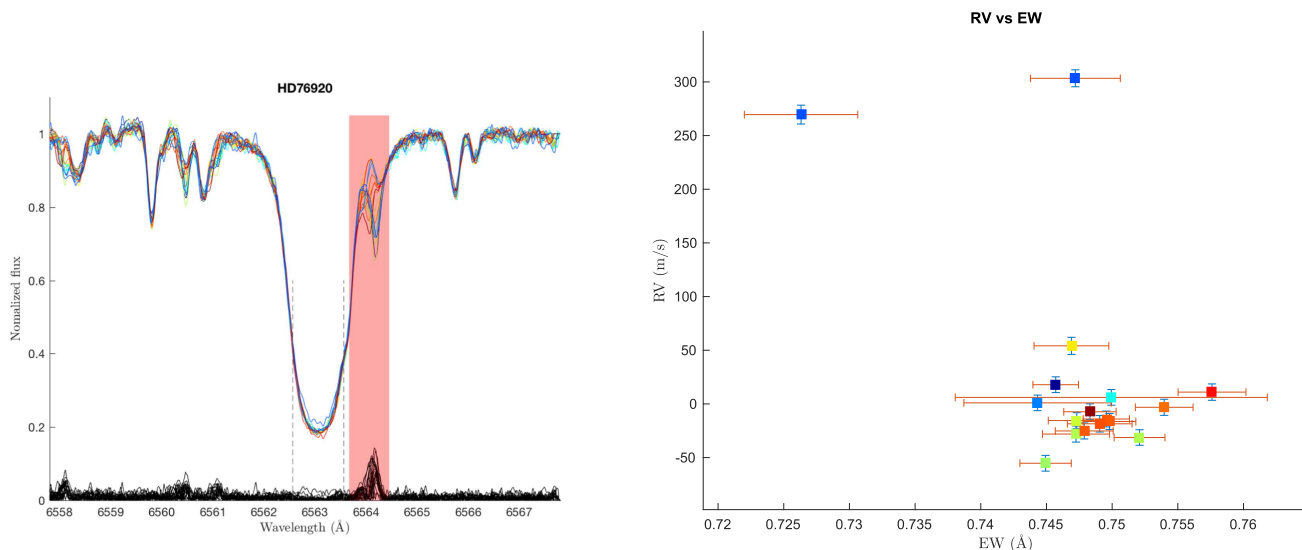


Figure 8. Left: the stacked normalized H α line from UCLES observations. The H α region is labeled within the black dashed lines, whereas the telluric region is highlighted in the red shaded area. Below are the residual amplitudes from the template (constructed as the weighted average of all observations). Large residuals are due to telluric contamination. Right: radial velocity vs. H α equivalent width. The same epochs are presented in identical colors across these two panels, and the closeness in colors within the same panel represents the closeness in BJD.

the upper right quadrant of Figure 4 (i.e., highly eccentric planets that do not make particularly close approaches) is most likely an observational bias. That is, a highly eccentric planet on such an orbit would exhibit a radial velocity curve that is comparatively flat for most of the orbital cycle (e.g., Figure 1). Such a target would be downgraded in observing priority,

further diminishing the probability of catching the large velocity excursion that reveals the planet’s existence.

HD 76920b moves on an orbit that brings the planet within ~ 5 stellar radii of its host star (i.e., 4 stellar radii from the surface). While this is a close approach, it is not the closest known; that honor falls to 4 UMa b (Döllinger et al. 2007),

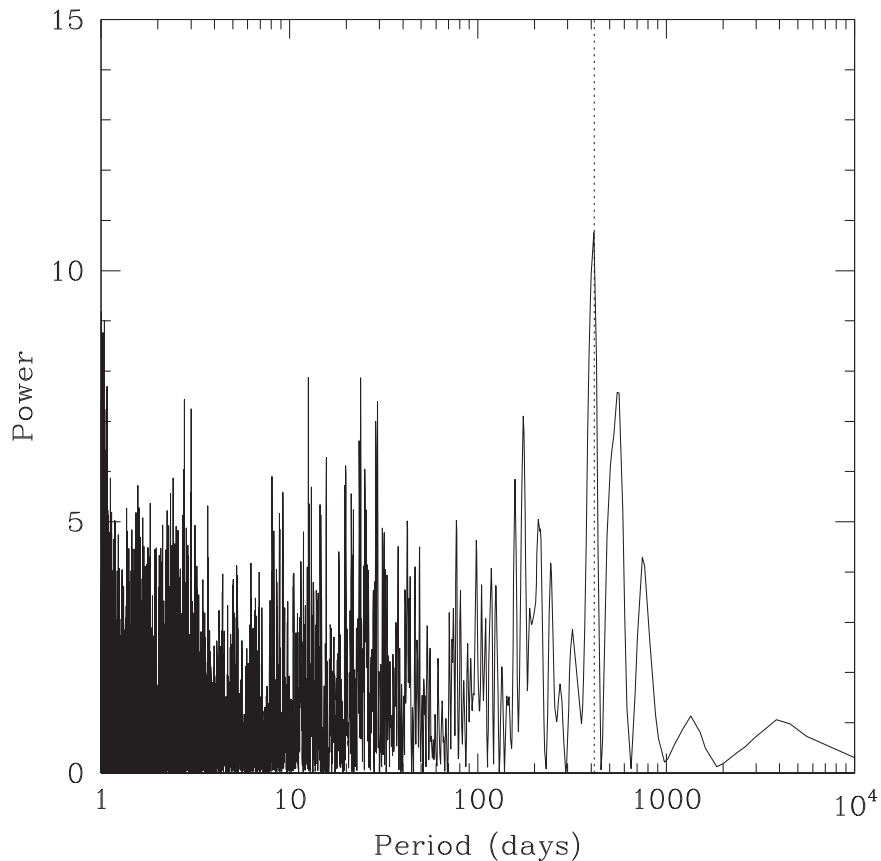


Figure 9. Periodogram of the radial velocity data for HD 76920 with the three velocity extrema removed. The signal of the planet remains, with a false-alarm probability of 0.6%.

which comes in to about 2 stellar radii of the surface of its host. The estimated radii for these evolved stars are model-dependent and are fraught with uncertainties not reflected in Figure 4. Hence, the exact values are less important than the overall message, which is that highly eccentric planets orbiting evolved stars make close approaches and are thus valuable laboratories for studying star–planet interactions.

The origin of highly eccentric planets is often attributed to the Kozai–Lidov mechanism (Kozai 1962; Lidov 1962), whereby a binary stellar companion orbiting at $i \gtrsim 39^\circ$ relative to the planet exchanges eccentricity and inclination with the planet, driving large excursions in planetary eccentricity. This is likely the case for the two best-known extremely eccentric planets: HD 20782b (Jones et al. 2006; Kane et al. 2016) and HD 80606b (Naef et al. 2001; Wittenmyer et al. 2007), both of which are in systems containing a binary stellar companion. However, we see no evidence for such a companion in the HD 76920 system: there is no residual radial velocity trend, and no candidate stellar companions are visible within 5 arcminutes.

Frewen & Hansen (2016) studied the influence of Kozai–Lidov oscillations to explain the lack of warm Jupiters around evolved stars. They found that such oscillations efficiently remove warm Jupiters, showing that by the time the expanding star reaches $R > 5 R_\odot$, no planet has survived engulfment, while an identical constant eccentricity population survives beyond $40 R_\odot$. Although simulations of Kozai–Lidov oscillations are not available for the orbital distance of HD 76920, the results of Frewen & Hansen (2016), and the fact that no stellar companion is found orbiting HD 76920, suggest that Kozai

migration is unlikely to be the origin of the observed eccentricity. While capture of a free-floating planet is possible, such events typically emplace the captured body on very wide orbits. For example, simulations by Parker et al. (2017) show that free-floating planets are exclusively captured onto orbits with $a > 100$ au. It is unlikely that stellar perturbations could reduce the semimajor axis by 2–3 orders of magnitude. A past episode of planet–planet scattering offers an alternative: high eccentricities can be attained in systems that eject one or more comparable-mass planets. In such systems, often a second planet is retained on a wide (10–100 au) orbit (e.g., Chatterjee et al. 2008; Mustill et al. 2014; Götberg et al. 2016), which may escape detection in the current RV data.

4.1. Transit Probability

If a highly eccentric gas giant happens to transit, it becomes all the more valuable, as it will offer a unique window into the physics and composition of “cold Jupiters.” At present, only one such planet is known, HD 80606b, with $e = 0.93$ and an orbital period of 111 days. It was discovered to transit in 2009 (Fossey et al. 2009; Garcia-Melendo & McCullough 2009; Moutou et al. 2009), and the transit was further characterized in a multi-site ground-based observing campaign by Winn et al. (2009). A *Spitzer* campaign centered on the periastron passage (Laughlin et al. 2009) allowed for the direct measurement of the atmospheric heating due to the ~ 30 hr close approach. For comparison, HD 80606b passes to within 5.5 stellar radii of the star’s surface at its closest approach (compared to 4 host-star radii for HD 76920b).

The eccentricity of planetary orbits can have a major impact on the expected transit properties of the planet (Barnes 2007; Kane & von Braun 2008). The eccentric nature of the HD 76920 b planetary orbit, combined with the relatively large size of the host star (see Table 2), make this planet an intriguing prospect for transit observations. A similar case was studied by Kane et al. (2010) for the planet orbiting iota Draconis. In that case, the eccentricity is smaller, but the star is larger and the periastron passage of the planet occurs very close to inferior conjunction (where the true anomaly $f \sim 0^\circ$). By contrast, the orbital fit from Table 3 and the orbit visualization shown in Figure 3 demonstrate that inferior conjunction for HD 76920 b occurs at a true anomaly of $f \sim 90^\circ$. At this location in its orbit, the star–planet separation will be 0.342 au, where the calculated orbital velocity of the planet will be a factor of 1.85 larger than the Earth’s orbital velocity. The net effect of these factors is to produce a transit probability of 10.3% and a transit duration of 2.3 days, assuming a Jovian planetary radius. By comparison, if the planet were in a circular orbit with the same semimajor axis of $a = 1.1491$ au, then the transit probability would be 3.1% and the transit duration would be ~ 4 days. The relatively large transit duration makes this a difficult observation from the ground, but the most difficult aspect is the small predicted transit depth of 0.02% resulting from the large stellar radius. The combination of transit probability and depth means that transiting giant planets around giant stars are likely plentiful but few have been detected. Currently, the largest stars ($R_* = 6.3 R_\odot$) for which a planet has been detected are Kepler-91 (Lillo-Box et al. 2014) and TYC 3667-1280-1 (Niedzielski et al. 2016). Precision space-based photometry of giant stars will provide valuable information for the mass–radius relationship of giant planets around evolved stars. These opportunities will be provided by TESS (Ricker et al. 2014) and CHEOPS (Broeg et al. 2013).

4.2. Circumstellar Matter

In Wittenmyer et al. (2017b), we investigated the possibility of debris disks orbiting the giant stars HD 86950 and HD 29399, both of which were identified by McDonald et al. (2012) as having a possible infrared excess based on the presence of excess emission at $9 \mu\text{m}$ in the AKARI/IRC All-Sky Survey (Ishihara et al. 2010). Because McDonald et al. (2012) also noted an infrared excess for HD 76920 with a fractional luminosity ($L_{\text{dust}}/L_{\text{star}}$) of $\sim 1.2 \times 10^{-3}$ peaking at $12 \mu\text{m}$, we undertook a similar analysis in this work. We compiled a spectral energy distribution from photometry spanning optical to mid-infrared wavelengths, including optical *BV*, near-infrared 2MASS *JHK_s* (Skrutskie et al. 2006), *WISE* (Wright et al. 2010), AKARI $9 \mu\text{m}$ (Ishihara et al. 2010), and the IRAS faint source catalog (Moshir et al. 1990). We illustrate the stellar photospheric emission with a model from the BT-SETTL/Nextgen (Allard et al. 2012) stellar atmospheres grid appropriate for the spectral type (K0 III; $T_{\text{eff}} = 4700$ K, $\log g = 3.0$, $[\text{Fe}/\text{H}] = 0.0$), and scaled to the stellar radius and TGAS distance (Gaia Collaboration et al. 2016; Wittenmyer et al. 2016c). We color-corrected the AKARI and WISE flux densities assuming blackbody emission from the star. The resulting spectral energy distribution is shown in Figure 10. No significant evidence of infrared excess is present. The infrared excess noted in McDonald et al. (2012) is based on AKARI $9 \mu\text{m}$, IRAS $12 \mu\text{m}$, and IRAS $25 \mu\text{m}$ data points. We have added WISE 3 and WISE 4 photometry to that mix.

No evidence of significant excess from the target is present after color correction of data points (IRAS12, IRAS25 have $K = 1.4$ for a 5000 K blackbody) and the calibration uncertainties of WISE 3 and 4 ($\sim 5\%$ and 6% , respectively) are taken into account.

4.3. Tidal Effects and Doomed Worlds

Planet–star tidal interactions become very strong when stars leave the main sequence. The increase in stellar radius means that the planet’s gravity can more easily deform the star, and the star’s deep convective envelope is highly efficient at dissipating the energy required for this deformation. The result is a damping of the planet’s orbital semimajor axis and eccentricity. The dominance of the tide raised on the star and the large stellar moment of inertia, mean that the planetary semimajor axis and eccentricity can continue to decay until the star engulfs the planet. This contrasts with the case of an eccentric planet orbiting a main-sequence star, for which the tide raised on the planet usually dominates, and the eccentricity decays to zero at a non-zero semimajor axis (see Figure 8 of Villaver et al. 2014). Engulfment of the planet by the star is also aided by the rapidly expanding stellar radius. Working against this, as the star ascends the red giant branch (RGB), stellar mass loss begins to accelerate, causing the planet’s orbit to expand. The fate of the planet thus depends on the stellar radius expansion, tidal forces dragging the planet inwards, and mass loss moving the planet out. The high eccentricity and modest semimajor axis of HD 76920b mean that it is likely to be ingested by its host star as the latter ascends the RGB.

We model the future evolution of HD 76920b using the method presented in (Villaver et al. 2014). This uses the tidal model of Zahn (1977) for the tide raised on the star, which is suitable for highly convective RGB stars, and (Matsumura et al. 2010) for the tide raised on the planet. First, we run a reference grid of planets at a range of semimajor axes (0.1–10 au) and eccentricities (0–0.95) orbiting a $1.17 M_\odot$ star (from SSE, Hurley et al. 2000). The mass of the planets is $4 M_{\text{Jup}}$. Their trajectories (after the first 1 Gyr, during which planets at the top left circularise quickly) in $a - e$ space are shown in Figure 11 as faint lines. Evolution along the main sequence is shown in gray, while evolution along the subgiant branch and RGB is shown in light brown. Many more planets are affected by tides on the RGB than on the MS. Two tracks starting close to the present orbit of HD 76920b are highlighted. These tracks predict a modest decay of semimajor axis and eccentricity before the planet is engulfed in a little under 100 Myr. Figure 4 shows the periastron distance in terms of the stellar radius. The periastron of HD 76920b is at 4.82 times the stellar radius. Note that at $r_p/R_* \approx 2-3$, planets are in jeopardy (Villaver et al. 2014) as that is where the tidal force starts to dominate the orbital evolution. The star HD 76920 still has to evolve a bit up the red giant branch in order to tidally catch the planet at periastron.

While this planet will certainly end up engulfed by its host star, being too close for stellar mass loss to win over tidal orbital decay, making an exact prediction of its future evolution is challenging, partly because of the uncertainties in modeling tidal forces and partly because of uncertainties on the stellar and planetary mass. As an example, dropping the stellar mass to $1.1 M_\odot$ results in much stronger eccentricity decay before engulfment, with eccentricities dropping to around 0.7 at the time of engulfment. The high sensitivity of stellar evolutionary

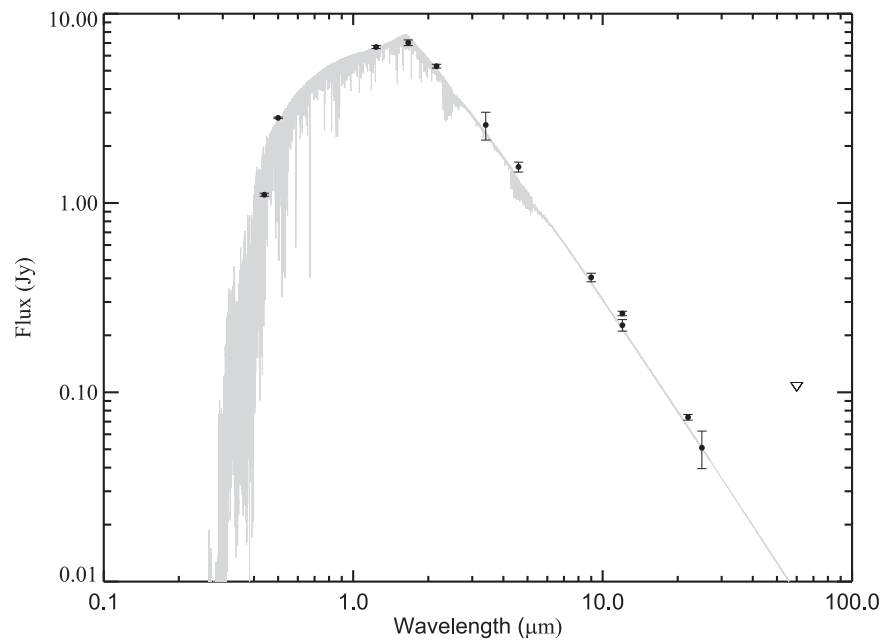


Figure 10. Spectral energy distribution of HD 76920. The photometric data compiled from literature sources are shown as open black diamonds, with 1σ uncertainties. The triangle at $60\ \mu\text{m}$ is an upper limit from IRAS. The stellar photosphere model is shown in gray and has been scaled according to the assumed stellar radius and parallax-derived distance (i.e., it is not a least-squares fit to the photometry). No significant evidence of infrared excess is present, save for marginal 3σ excesses in the *WISE* 3 and 4 bands.

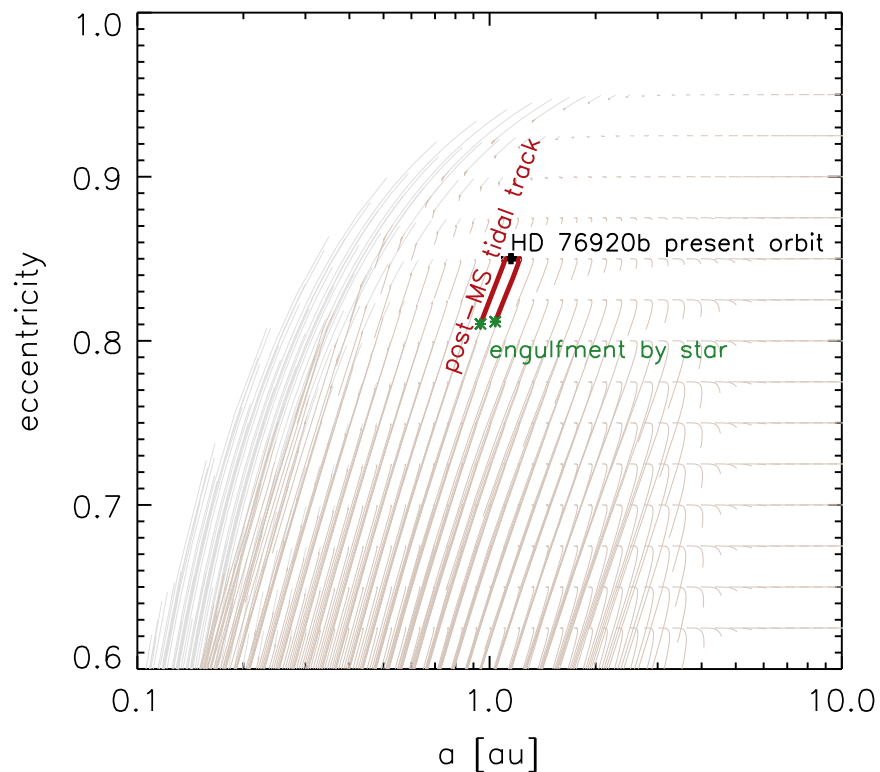


Figure 11. Tidal evolution of planets orbiting a $1.17\ M_{\odot}$ star. Evolution along the main sequence is shown in gray, and evolution along the subgiant and RGB stages is shown in light brown. Two trajectories near the present location of HD 76920b are highlighted. These end in engulfment by the swelling RGB star is around 100 Myr.

timescales on stellar mass means that at lower stellar masses, there is more time for tidal decay to work to shrink the orbit before planetary engulfment.

The tracks shown in Figure 11 use solar metallicity, while HD 76920 has $[\text{Fe}/\text{H}] = -0.11$. This introduces another source of uncertainty in the calculation of the decay timescales.

The evolution of the star at a slightly lower metallicity than the one computed here is equivalent to the evolution of a more massive stellar mass at solar metallicity. HD 76920 would in that case evolve a bit faster than is assumed in Figure 11 and thus will move more quickly into the stellar envelope. Also note that mass loss is expected to be affected by the metallicity

of the star, and although red giant mass-loss rates are not very prominent, they still have an effect in the final outcome of planetary systems (see Villaver et al. 2014).




4.4. Future Work

Fortuitous observations have enabled us to characterize the orbit of HD 76920b as being unambiguously eccentric. That is, the values of e and ω have produced a radial velocity curve that cannot be mimicked by two low-eccentricity planets, a pathology that is distinctly possible when observations are sparse and poorly sampled (e.g., Shen & Turner 2008; Anglada-Escudé et al. 2010; Wittenmyer et al. 2012, 2013b). It would of course be desirable to achieve better phase coverage of the critical velocity excursion at periastron passage, to obtain a more precise measurement of the radial velocity amplitude (and hence the planet's mass). We predict the next such passage to occur on 2018 January 17 (BJD 2458136.3 \pm 0.5), with \sim 30 days of significant acceleration on either side of the velocity maximum. Interested observers with dedicated (e.g., MINERVA: Swift et al. 2015) or queue-scheduled (e.g., CHIRON) telescope resources are highly encouraged to make plans to characterize the orbit of HD 76920b at that time. Endl et al. (2006) used the Hobby-Eberly Telescope in this manner to make high-cadence measurements of the periastron passage of HD 45350b, an $e = 0.76$ planet exhibiting a radial velocity curve similar to that of HD 76920b. Likewise, high-cadence observations capturing the periastron passage of HD 37605b enabled Cochran et al. (2004) to confirm the highly eccentric planet ($e = 0.737$). These examples highlight the importance of flexibly scheduled radial velocity observations for truly understanding the orbital properties of unusual planets such as HD 76920b.

We gratefully acknowledge the efforts of PPPS guest observers Brad Carter, Hugh Jones, and Simon O'Toole. A.J.M. is supported by the Knut and Alice Wallenberg Foundation. J.S.J. acknowledges support by Fondecyt grant 1161218 and partial support by CATA-Basal (PB06, CONICYT). E.V. acknowledges support from the Spanish Ministerio de Economía y Competitividad under grant AYA2014-55840P. This work has made use of data from the European Space Agency (ESA) mission *Gaia* (<https://www.cosmos.esa.int/gaia>), processed by the *Gaia* Data Processing and Analysis Consortium (DPAC, <https://www.cosmos.esa.int/web/gaia/dpac/consortium>). Funding for the DPAC has been provided by national institutions, in particular the institutions participating in the *Gaia* Multilateral Agreement. This research has made use of NASA's Astrophysics Data System (ADS), and the SIMBAD database, operated at CDS, Strasbourg, France. This research has made use of the Spanish Virtual Observatory (<http://svo.cab.inta-csic.es>) supported from the Spanish MINECO through grant AyA2014-55216. This research has also made use of the Exoplanet Orbit Database and the Exoplanet Data Explorer at exoplanets.org (Wright et al. 2011; Han et al. 2014).

Software: MOOG (Snedden 1973), Kurucz ATLAS9 (Castelli & Kurucz 2004), SSE (Hurley et al. 2000), emcee (Foreman-Mackey et al. 2013).

ORCID iDs

Robert A. Wittenmyer  <https://orcid.org/0000-0001-9957-9304>
 Jonathan Horner  <https://orcid.org/0000-0002-1160-7970>
 Stephen R. Kane  <https://orcid.org/0000-0002-7084-0529>
 J. P. Marshall  <https://orcid.org/0000-0001-6208-1801>
 J. S. Jenkins  <https://orcid.org/0000-0003-2733-8725>
 Eva Villaver  <https://orcid.org/0000-0003-4936-9418>
 R. P. Butler  <https://orcid.org/0000-0003-1305-3761>

References

- Addison, B. C., Tinney, C. G., Wright, D. J., et al. 2013, *ApJL*, 774, L9
 Allard, F., Homeier, D., & Freytag, B. 2012, *RSPTA*, 370, 2765
 Anderson, D. R., Smith, A. M. S., Lanotte, A. A., et al. 2011, *MNRAS*, 416, 2108
 Anglada-Escudé, G., López-Morales, M., & Chambers, J. E. 2010, *ApJ*, 709, 168
 Bailer-Jones, C. A. L. 2011, *MNRAS*, 411, 435
 Bakos, G. Á., Hartman, J., Torres, G., et al. 2011, *ApJ*, 742, 116
 Baluev, R. V. 2013, *MNRAS*, 436, 807
 Baranne, A., Queloz, D., Mayor, M., et al. 1996, *A&AS*, 119, 373
 Barnes, J. W. 2007, *PASP*, 119, 986
 Brahm, R., Jordán, A., & Espinoza, N. 2017, *PASP*, 129, 034002
 Broeg, C., Fortier, A., Ehrenreich, D., et al. 2013, in European Physical Journal Web of Conf. 47, Hot Planets and Cool Stars (Garching: ESO), 03005
 Burke, C. J. 2008, *ApJ*, 679, 1566
 Butler, R. P., Marcy, G. W., Williams, E., et al. 1996, *PASP*, 108, 500
 Butler, R. P., Wright, J. T., Marcy, G. W., et al. 2006, *ApJ*, 646, 505
 Castelli, F., & Kurucz, R. L. 2004, in IAU Symp. 210, Modelling of Stellar Atmospheres, ed. N. Piskunov et al. (Cambridge: Cambridge Univ. Press), A20
 Chatterjee, S., Ford, E. B., Matsumura, S., & Rasio, F. A. 2008, *ApJ*, 686, 580
 Cochran, W. D., Endl, M., McArthur, B., et al. 2004, *ApJL*, 611, L133
 de León, J., Campins, H., Tsiganis, K., Morbidelli, A., & Licandro, J. 2010, *A&A*, 513, A26
 Diego, F., Charalambous, A., Fish, A. C., & Walker, D. D. 1990, *Proc. SPIE*, 1235, 562
 Döllinger, M. P., Hatzes, A. P., Pasquini, L., et al. 2007, *A&A*, 472, 649
 Endl, M., Brugamyer, E. J., Cochran, W. D., et al. 2016, *ApJ*, 818, 34
 Endl, M., Cochran, W. D., Wittenmyer, R. A., & Hatzes, A. P. 2006, *AJ*, 131, 3131
 Feng, F., Tuomi, M., & Jones, H. R. A. 2017, *MNRAS*, 470, 4794
 Foreman-Mackey, D., Hogg, D. W., Lang, D., & Goodman, J. 2013, *PASP*, 125, 306
 Fossey, S. J., Waldmann, I. P., & Kipping, D. M. 2009, *MNRAS*, 396, L16
 Frewen, S. F. N., & Hansen, B. M. S. 2016, *MNRAS*, 455, 1538
 Gaia Collaboration, Brown, A. G. A., Vallenari, A., et al. 2016, *A&A*, 595, A2
 Garcia-Melendo, E., & McCullough, P. R. 2009, *ApJ*, 698, 558
 Gaudi, B. S., Seager, S., & Mallen-Ornelas, G. 2005, *ApJ*, 623, 472
 Göteborg, Y., Davies, M. B., Mustill, A. J., Johansen, A., & Church, R. P. 2016, *A&A*, 592, A147
 Gregory, P. C. 2005, *ApJ*, 631, 1198
 Han, E., Wang, S. X., Wright, J. T., et al. 2014, *PASP*, 126, 827
 Hinse, T. C., Horner, J., & Wittenmyer, R. A. 2014, *JASS*, 31, 187
 Høg, E., Fabricius, C., Makarov, V. V., et al. 2000, *A&A*, 355, L27
 Horner, J., Evans, N. W., & Bailey, M. E. 2004, *MNRAS*, 354, 798
 Horner, J., Evans, N. W., Bailey, M. E., & Asher, D. J. 2003, *MNRAS*, 343, 1057
 Horner, J., Marshall, J. P., Wittenmyer, R. A., & Tinney, C. G. 2011, *MNRAS*, 416, L11
 Horner, J., Wittenmyer, R. A., Hinse, T. C., et al. 2013, *MNRAS*, 435, 2033
 Houk, N., & Cowley, A. P. (ed.) 1975, University of Michigan Catalogue of Two-dimensional Spectral Types for the HD Stars, Vol. I. Declinations -90 to -53 (Ann Arbor, MI: Department of Astronomy, University of Michigan), 19
 Howard, A. W., Marcy, G. W., Johnson, J. A., et al. 2010, *Sci*, 330, 653
 Huber, D., Carter, J. A., Barbieri, M., et al. 2013, *Sci*, 342, 331
 Hurley, J. R., Pols, O. R., & Tout, C. A. 2000, *MNRAS*, 315, 543
 Ishihara, D., Onaka, T., Katata, H., et al. 2010, *A&A*, 514, A1
 Jenkins, J. S., Jones, H. R. A., Tuomi, M., et al. 2017, *MNRAS*, 466, 443
 Jenkins, J. S., & Tuomi, M. 2014, *ApJ*, 794, 110

- Jenkins, J. S., Tuomi, M., Brasser, R., Ivanyuk, O., & Murgas, F. 2013, *ApJ*, **771**, 41
- Johnson, J. A., Aller, K. M., Howard, A. W., & Crepp, J. R. 2010, *PASP*, **122**, 905
- Johnson, J. A., Clanton, C., Howard, A. W., et al. 2011, *ApJS*, **197**, 26
- Johnson, J. A., Fischer, D. A., Marcy, G. W., et al. 2007, *ApJ*, **665**, 785
- Jones, H. R. A., Butler, R. P., Tinney, C. G., et al. 2006, *MNRAS*, **369**, 249
- Jones, M. I., Brahm, R., Wittenmyer, R. A., et al. 2017, *A&A*, **602**, A58
- Jones, M. I., Jenkins, J. S., Brahm, R., et al. 2016, *A&A*, **590**, A38
- Jones, M. I., Jenkins, J. S., Rojo, P., & Melo, C. H. F. 2011, *A&A*, **536**, A71
- Kane, S. R., Reffert, S., Henry, G. W., et al. 2010, *ApJ*, **720**, 1644
- Kane, S. R., & von Braun, K. 2008, *ApJ*, **689**, 492
- Kane, S. R., Wittenmyer, R. A., Hinkel, N. R., et al. 2016, *ApJ*, **821**, 65
- Kaufer, A., Stahl, O., Tubbesing, S., et al. 1999, *Msngr*, **95**, 8
- Knutson, H. A., Fulton, B. J., Montet, B. T., et al. 2014, *ApJ*, **785**, 126
- Kozai, Y. 1962, *AJ*, **67**, 591
- Laughlin, G., Deming, D., Langton, J., et al. 2009, *Natur*, **457**, 562
- Levison, H. F., Terrell, D., Wiegert, P. A., Dones, L., & Duncan, M. J. 2006, *Icar*, **182**, 161
- Lidov, M. L. 1962, *P&SS*, **9**, 719
- Lillo-Box, J., Barrado, D., Moya, A., et al. 2014, *A&A*, **562**, A109
- Lissauer, J. J. 1993, *ARA&A*, **31**, 129
- Liu, M. C., Magnier, E. A., Deacon, N. R., et al. 2013, *ApJL*, **777**, L20
- Lopez, E. D., & Fortney, J. J. 2014, *ApJ*, **792**, 1
- Lucas, P. W., & Roche, P. F. 2000, *MNRAS*, **314**, 858
- Maldonado, J., Villaver, E., & Eiroa, C. 2013, *A&A*, **554**, A84
- Marcy, G. W., Isaacson, H., Howard, A. W., et al. 2014, *ApJS*, **210**, 20
- Martínez-Arnáiz, R., Maldonado, J., Montes, D., Eiroa, C., & Montesinos, B. 2010, *A&A*, **520**, A79
- Masuda, K. 2014, *ApJ*, **783**, 53
- Matsumura, S., Peale, S. J., & Rasio, F. A. 2010, *ApJ*, **725**, 1995
- Mayor, M., & Queloz, D. 1995, *Natur*, **378**, 355
- McDonald, I., Zijlstra, A. A., & Boyer, M. L. 2012, *MNRAS*, **427**, 343
- Meschiari, S., Wolf, A. S., Rivera, E., et al. 2009, *PASP*, **121**, 1016
- Moshir, M., Kopan, G., Conrow, T., et al. 1990, *BAAS*, **22**, 1325
- Moutou, C., Hébrard, G., Bouchy, F., et al. 2009, *A&A*, **498**, L5
- Mustill, A. J., Veras, D., & Villaver, E. 2014, *MNRAS*, **437**, 1404
- Naef, D., Latham, D. W., Mayor, M., et al. 2001, *A&A*, **375**, L27
- Niedzielski, A., Villaver, E., Nowak, G., et al. 2016, *A&A*, **589**, L1
- Niedzielski, A., Villaver, E., Wolszczan, A., et al. 2015, *A&A*, **573**, A36
- Parker, R. J., Lichtenberg, T., & Quanz, S. P. 2017, *MNRAS Letters*, in press, arXiv:1709.00418
- Pepper, J., Rodriguez, J. E., Collins, K. A., et al. 2017, *AJ*, **153**, 215
- Pojmanski, G. 1997, *AcA*, **47**, 467
- Reffert, S., Bergmann, C., Quirrenbach, A., Trifonov, T., & Künstler, A. 2015, *A&A*, **574**, A116
- Ricker, G. R., Winn, J. N., Vanderspek, R., et al. 2014, *Proc. SPIE*, **9143**, 914320
- Robertson, P., Mahadevan, S., Endl, M., & Roy, A. 2014, *Sci*, **345**, 440
- Rogers, L. A. 2015, *ApJ*, **801**, 41
- Shen, Y., & Turner, E. L. 2008, *ApJ*, **685**, 553
- Sinukoff, E., Howard, A. W., Petigura, E. A., et al. 2016, *ApJ*, **827**, 78
- Skrutskie, M. F., Cutri, R. M., Stiening, R., et al. 2006, *AJ*, **131**, 1163
- Snedden, C. 1973, *ApJ*, **184**, 839
- Steel, D. I., Asher, D. J., & Clube, S. V. M. 1991, *MNRAS*, **251**, 632
- Sumi, T., Kamiya, K., Bennett, D. P., et al. 2011, *Natur*, **473**, 349
- Swift, J. J., Bottom, M., Johnson, J. A., et al. 2015, *JATIS*, **1**, 027002
- Tamaz, O., Ségransan, D., Udry, S., et al. 2008, *A&A*, **480**, L33
- Tinney, C. G., Butler, R. P., Marcy, G. W., et al. 2001, *ApJ*, **551**, 507
- Tokovinin, A., Fischer, D. A., Bonati, M., et al. 2013, *PASP*, **125**, 1336
- Triaud, A. H. M. J., Collier Cameron, A., Queloz, D., et al. 2010, *A&A*, **524**, A25
- Tuomi, M., Jones, H. R. A., Jenkins, J. S., et al. 2013, *A&A*, **551**, A79
- Valenti, J. A., Butler, R. P., & Marcy, G. W. 1995, *PASP*, **107**, 966
- Villaver, E., Livio, M., Mustill, A. J., & Siess, L. 2014, *ApJ*, **794**, 3
- Williams, I. P., & Wu, Z. 1993, *MNRAS*, **262**, 231
- Winn, J. N., Howard, A. W., Johnson, J. A., et al. 2009, *ApJ*, **703**, 2091
- Wittenmyer, R. A., Butler, R. P., Tinney, C. G., et al. 2016a, *ApJ*, **819**, 28
- Wittenmyer, R. A., Endl, M., Cochran, W. D., & Levison, H. F. 2007, *AJ*, **134**, 1276
- Wittenmyer, R. A., Endl, M., Wang, L., et al. 2011a, *ApJ*, **743**, 184
- Wittenmyer, R. A., Horner, J., & Marshall, J. P. 2013a, *MNRAS*, **431**, 2150
- Wittenmyer, R. A., Horner, J., Mengel, M. W., et al. 2017a, *AJ*, **153**, 167
- Wittenmyer, R. A., Horner, J., Tuomi, M., et al. 2012, *ApJ*, **753**, 169
- Wittenmyer, R. A., Johnson, J. A., Butler, R. P., et al. 2016b, *ApJ*, **818**, 35
- Wittenmyer, R. A., Jones, M. I., Zhao, J., et al. 2017b, *AJ*, **153**, 51
- Wittenmyer, R. A., Liu, F., Wang, L., et al. 2016c, *AJ*, **152**, 19
- Wittenmyer, R. A., Tinney, C. G., Butler, R. P., et al. 2011b, *ApJ*, **738**, 81
- Wittenmyer, R. A., Wang, L., Liu, F., et al. 2015, *ApJ*, **800**, 74
- Wittenmyer, R. A., Wang, S., Horner, J., et al. 2013b, *ApJS*, **208**, 2
- Wolfgang, A., & Lopez, E. 2015, *ApJ*, **806**, 183
- Wright, E. L., Eisenhardt, P. R. M., Mainzer, A. K., et al. 2010, *AJ*, **140**, 1868
- Wright, J. T., Fakhouri, O., Marcy, G. W., et al. 2011, *PASP*, **123**, 412
- Wright, J. T., Marcy, G. W., Howard, A. W., et al. 2012, *ApJ*, **753**, 160
- Zahn, J.-P. 1977, *A&A*, **57**, 383